Available online at www.sciencedirect.com
ScienceDirect
Journal of the European Ceramic Society 29 (2009) 595–601
www.elsevier.com/locate/jeurceramsoc

Sintered material from alkaline basaltic tuffs

Alexander Karamanov [a,*], Lorenzo Arrizza [b], Sibel Ergul [c]

[a] *Institute of Physical Chemistry, Bulgarian Academy of Sciences, G. Bonchev Str. Block 11, 1113 Sofia, Bulgaria*
[b] *Microscopy Centrum, University of L'Aquila, 67100, Monteluco di Roio – L'Aquila, Italy*
[c] *Department of Geological Engineering, University of Cukurova, 01330 Balcali, Adana, Turkey*

Received 26 February 2008; received in revised form 2 July 2008; accepted 9 July 2008
Available online 23 August 2008

Abstract

The possibility to obtain sintered material from alkaline basaltic tuffs is demonstrated. The parent rock was milled for 10–15 min, the resulting powder was pressed at 100 MPa and the obtained samples were heat-treated in the range of 1000–1140 °C. The sintering behaviour and the phase formation were studied by pycnometry, dilatometry, DTA, XRD and SEM.

The final material was obtained by sintering at 1100 °C and is characterized by zero water absorption, 8–9 vol.% closed porosity and a structure similar to a glass-ceramic. Due to high crystallization trend of used composition, phase formation takes place during the sintering and cooling steps; this leads to a crystallinity of ∼60% and formation of different crystal phases (pyroxene, anorthite, spinel and hematite).

Despite the low-cost production cycle the obtained material is characterized by high mechanical properties: bending strength of 100 MPa and Young modulus of 90 GPa.

Keywords: Igneous rocks; Sintering; Crystallization; Mechanical properties

1. Introduction

The re-fused rocks manufacture (petrurgy) was created in the beginning of the 20th Century as an independent branch of the silicate industry.[1] Nevertheless, several industrial units are yet active in different countries and effectively produce pavements, building tiles, pipes, bends and glassy insulation fibres (rock wool).[2–5]

Due to the high chemical durability of the natural basalts, which are the main raw materials for the petrurgy, iron-rich glass and glass-ceramic materials with basalt-like compositions were also developed for nuclear waste disposal[6–8] and for vitrification of various hazardous industrial wastes.[9–17]

The iron-rich silicate melts are characterized by low viscosity and an elevated crystallization trend, which allows production of polycrystalline materials applying short production cycles at low temperature. For these reasons, many researchers continue to study the melting and the crystallization behaviour of different igneous rocks and to characterize the obtained materials.[18–21] Other investigations are related to the possible utilization of some volcanic rocks as sintering promoters or glazes in the traditional ceramic industry.[22–24]

The basalt related igneous rocks are classified in two main groups: subalkaline and alkaline; the first group comprises tholeiitic and calcalkaline basalts, whereas the second includes alkaline and alkaline–olivine basalts.[25] As of today, petrurgy uses mainly tholeiitic basalts and diabasic rocks,[1,18–20,26,27] which, due to the higher $SiO_2 + Al_2O_3$ percentage, are characterized by a moderate crystallization trend.

On the contrary, the low viscosity alkaline basalts, because of their spontaneous crystallization, are inappropriate for a traditional petrurgical manufacture. In fact, when the crystallization ability is too high the increasing of apparent viscosity due to rapid phase formation causes difficulties during the forming process; moreover, the structure of material becomes inhomogeneous and coarse.

Similar low viscosity compositions, however, might be used to obtain sintered glass-ceramics. In fact, the sinter-crystallization technique, which is an alternative technology for the production of glass-ceramics, was successfully used for synthesis of several iron-rich sintered silicate materials.[28–31]

* Corresponding author. Tel.: +359 2 979 2552; fax: +359 2 971 2688.
E-mail address: karama@ipc.bas.bg (A. Karamanov).

0955-2219/$ – see front matter © 2008 Elsevier Ltd. All rights reserved.
doi:10.1016/j.jeurceramsoc.2008.07.002

Basalts exist as compact rocks and tuffs. The rocks are formed during slow cooling of lava, resulting in high crystallinity and hardness. Disintegration and milling of these rocks is quite difficult; hence, re-melting of basalts is carried out in special shaft furnaces working with crushed rock pieces with size of 10–20 cm.

Contrary, the basaltic tuffs are a result of intensive eruption and quick water or air cooling, leading to the formation of solids with high porosity and low crystallinity. Thus, crushing and milling of basaltic tuffs are very cheap and fast procedures.

In the present work tuffs with a typical alkaline–olivine composition are studied. The deposits of used rocks are located in Southern Anatolia and are estimated at about 1000 Mt. Their chemical and mineralogical compositions show negligible variations,[32] which is an important feature for their industrial application.

In our previous studies these tuffs were used for synthesis of ceramic[23] and sintered glass-ceramic materials.[31] The ceramic was obtained by mixing 50 wt.% tuffs with 50% local industrial clays, pressing at 30 MPa and sintering at 1150 °C. The glass-ceramic material was produced by re-melting at 1350 °C, milling of the resulting frits, pressing at 100 MPa and sinter-crystallization at 1080 °C.

The present work follows these studies and examines the possibility to obtain a low-cost material with improved mechanical properties and structure, similar to a sintered glass-ceramic, without re-melting of the tuffs and with no addition of clays.

The cost price of new material should be significantly lower than one of the "traditional" petrurgical materials and similar to that of the traditional tiling ceramic materials (as porcelain stoneware or earthenware). The last, however, are characterised by inferior mechanical properties and are produced at higher sintering temperature.

2. Experimental

The initial tuffs were crushed, milled for 10–15 min in agathe mill and the obtained powder was sieved under 75 μm. The chemical analysis, performed by XRF (Spectro XEPOS), evidences a typical alkaline–olivine basaltic composition (wt.%): SiO_2—43.18 ± 0.08, TiO_2—3.34 ± 0.01, P_2O_5—0.96 ± 0.03, Al_2O_3—13.15 ± 0.04, Fe_2O_3—13.49 ± 0.04, CaO—9.67 ± 0.05, MgO—8.48 ± 0.07, Na_2O—4.27 ± 0.19, K_2O—2.78 ± 0.01.

The tuffs powder was mixed and homogenized with 7.5% polyvinyl alcohol (PVA) solution in a ratio of 95/5 (wt.%); then "green" samples with initial sizes of 3/4/50 mm^3, 7/10/10 and 4/4/8 mm^3 were pressed at 100 MPa.

The crystallization and melting temperatures were evaluated by DTA technique (Linseiz L81) using 100 mg powder samples at heating rate of 10 °/C. The sintering of 4/4/8 mm^3 samples was studied at 10 °C/min by differential dilatometer (Netzsch 402 ED).

After drying at 110 °C and a 30 min heat-treatment at 270 °C (to eliminate the PVA), the 7/10/10 mm^3 samples were kept for 1 h at 1000, 1040, 1060, 1080, 1100, 1120 and 1140 °C (using heating and cooling rates of 10 °C/min). The apparent density, ρ, of obtained samples was measured by dry flow pycnometer (GeoPyc 1360). The skeleton, ρ_s, and absolute, ρ_a, densities were determined before and after milling the samples below 26 μm, respectively, using He displacement Pycnometer (AccuPyc 1330). The obtained values were used to calculate the total, P_T, closed, P_C, and open, P_O, porosities:

$$P_T = 100\frac{\rho_a - \rho}{\rho_a} \quad (1)$$

$$P_C = 100\frac{\rho_a - \rho_S}{\rho_a} \quad (2)$$

$$P_O = P_T - P_C \quad (3)$$

The phase composition of the sintered samples was characterized by X-ray diffraction analysis using powder samples (Philips PW1830, Cu Kα radiation). The data was recorded in the range of 10–80 2Θ at step of 0.02° and counting time of 6 s.

The crystalline fraction formed was estimated by comparing the intensity of the amorphous halo in the spectra of each of studied samples with that of corresponding basalt glass (obtained after re-melting at 1350 °C and water quenching[31]). This method is based on the assumption that the decrease in scattering intensity of the amorphous phase in partially crystallized samples is proportional to the amount of formed crystal phase.[33,34] In our study the crystallinity of each sample was obtained as an average of three measurements, carried out at 2Θ values of 25, 28 and 34, respectively.

The structure and morphology of the final material were investigated by Scanning Electron Microscopy (Philips XL30CP) using SE and BSE techniques. The chemical composition of surface and fracture of the final material, as well as of the formed crystal phases, was estimated by EDS analysis.

Series of 5 samples (initial size of 3/4/50 mm^3) was used to evaluate the mechanical properties of the material. The Young modulus was measured by means of non-destructive resonance frequency technique (GrindoSonic Mk5). The bending strength was evaluated by four point bending test at crosshead speed of 0.2 mm/min (Instron 1121 UTS).

Finally, the coefficient of linear thermal expansion (20–500 °C) was determined by Differential Dilatometer (Netzsch 402 ED) at 5 °C/min.

3. Results and discussion

3.1. Sintering and phase formation

Fig. 1 shows the DTA results (black line), together with the dilatometric sintering curve (grey line), whereas Fig. 2 presents the shrinkage rate as a function of temperature (i.e. first derivate of the sintering plot).

The DTA traces show a low intensity exothermal peak at 875 °C, which can be attributed to a secondary crystallization of the residual glassy phase, and large melting endothermal effect with onset temperature at ~1115 °C and peaks at 1160 and 1215 °C.

Due to the high amount of amorphous phase in parent tuffs the densification in dilatometric holder starts at ~715 °C and at

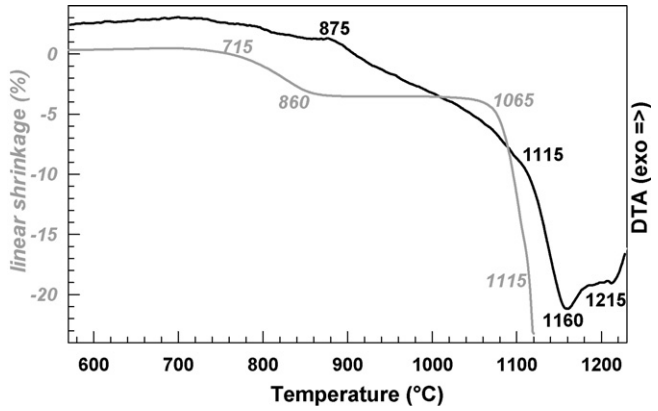

Fig. 1. Plots of dilatomertic sintering curve and DTA results vs. temperature.

~860 °C the linear shrinkage riches 3%. After that, however, the crystallization process inhibits the sintering and $\Delta L/L_0$ remains constant up to 1060 °C. At this temperature the densification process re-starts again and at 1100 °C the shrinkage becomes 16%. At higher temperatures the intense melting process and the load of the dilatometer push-road cause deformation of the sample.

The changes in sintering kinetics are presented in Fig. 2. It can be clearly seen that the densification rate in the low temperature interval starts to decrease already at 840 °C (i.e. with the beginning of secondary crystallization) and that the maximum sintering rate is achieved at 1100 °C. The beginning of swelling at 1110 °C is also remarkably distinguished.

Fig. 3 summarizes the variations in total, open and closed porosities after 1 h holding at different temperatures. The samples sintered at 1000, 1040 and 1060 °C are characterized by scarce densification, resulting in high percentage of open porosity, P_O, and no closed porosity, P_C. At 1080 °C, P_O decreases to ~17% and the formation of P_C starts. At 1100 and 1120 °C, no open porosity is detected, while the amount of closed porosity increases to 8–9 vol.%. The sample held at 1140 °C (not presented in the figure) shows overfiring and deformation.

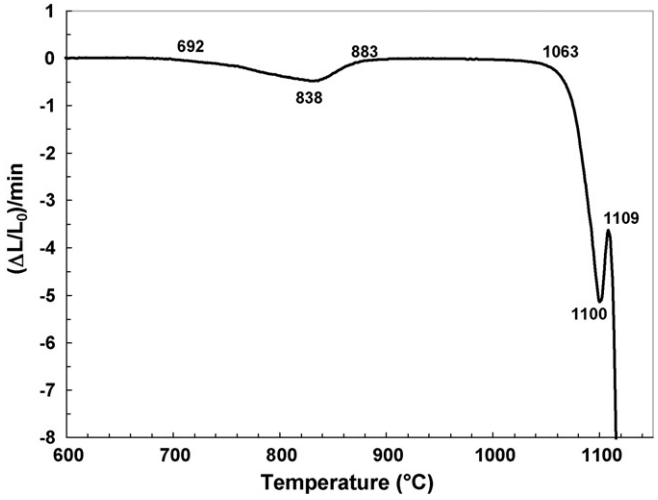

Fig. 2. Plot of the shrinkage rate vs. temperature.

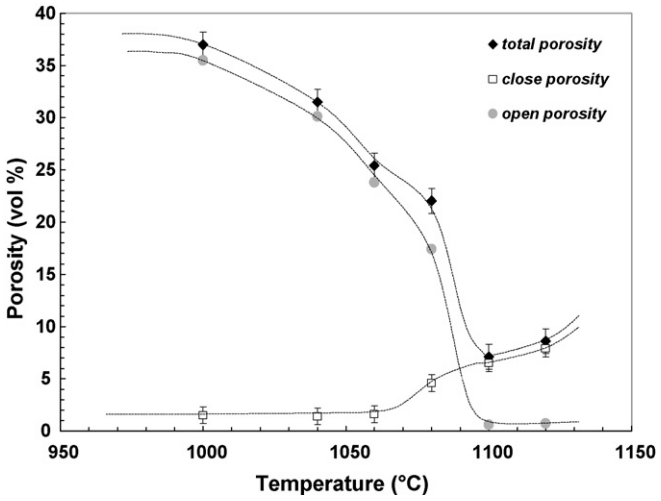

Fig. 3. Variation of total, open and closed porosities of samples, heat-treated for 1 h at different temperatures.

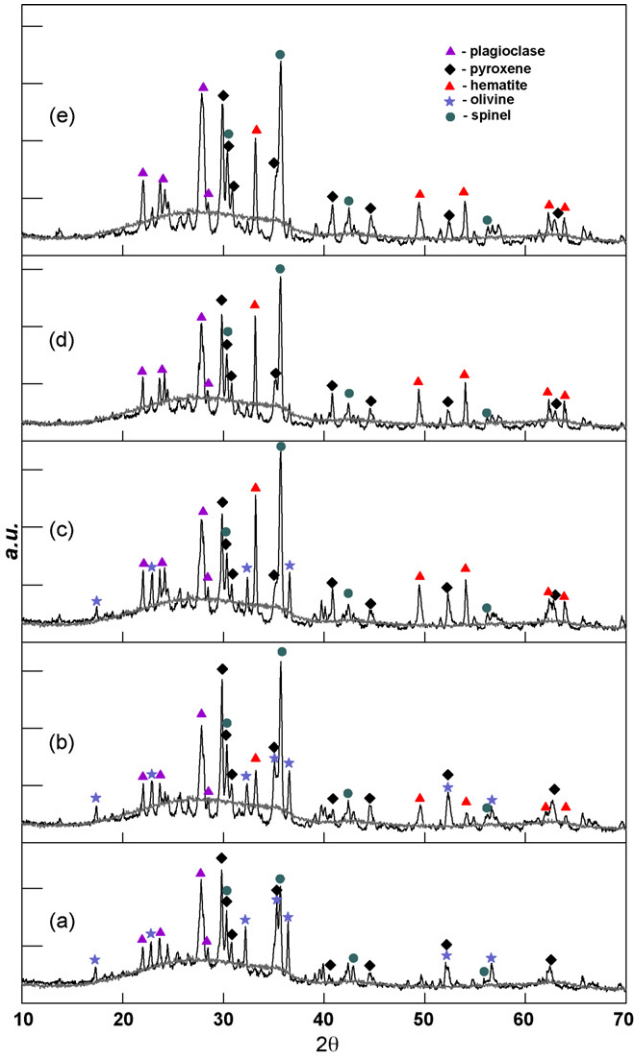

Fig. 4. XRD analysis results of parent tuffs (a) and samples obtained at different heat-treatments.

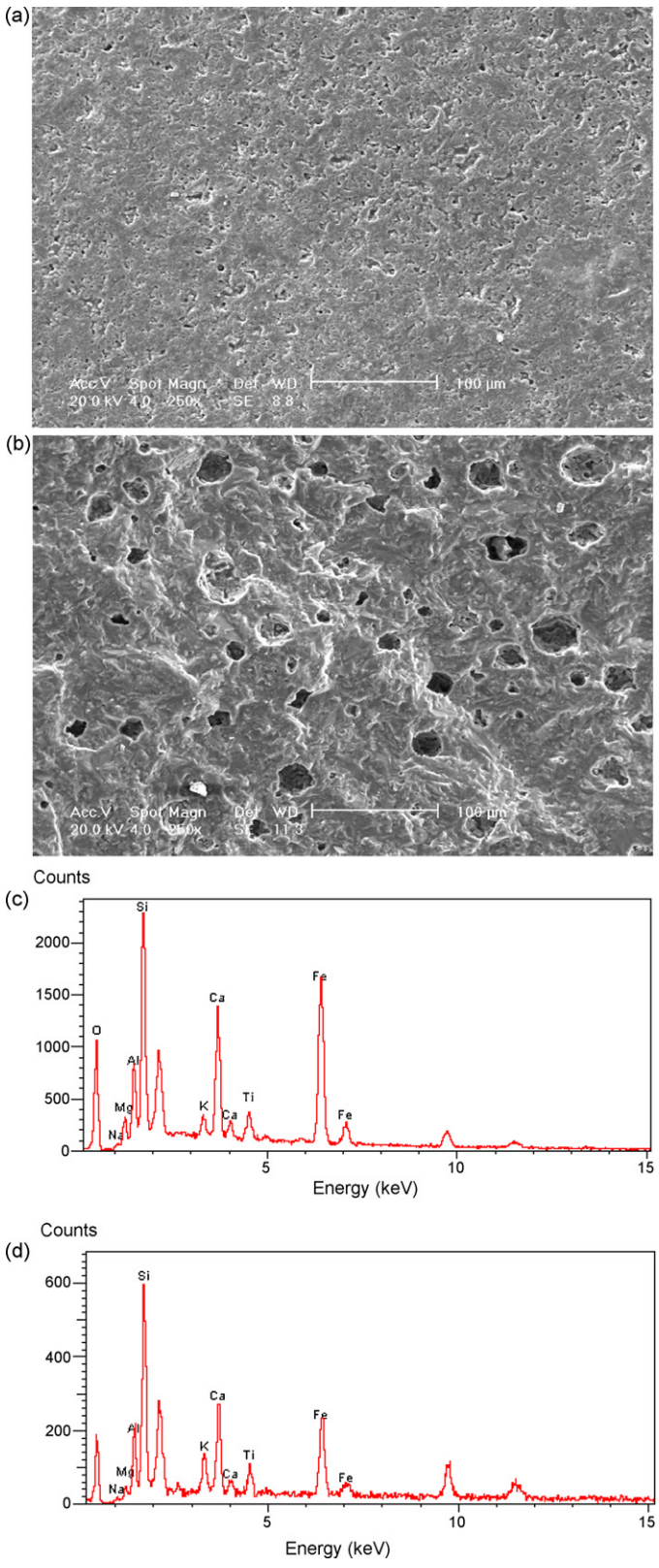

Fig. 5. SE-SEM images of the final material, obtained after 1 h at 1100 °C: surface (a) and fracture (b) with the corresponding EDS results (c) surface and (d) bulk.

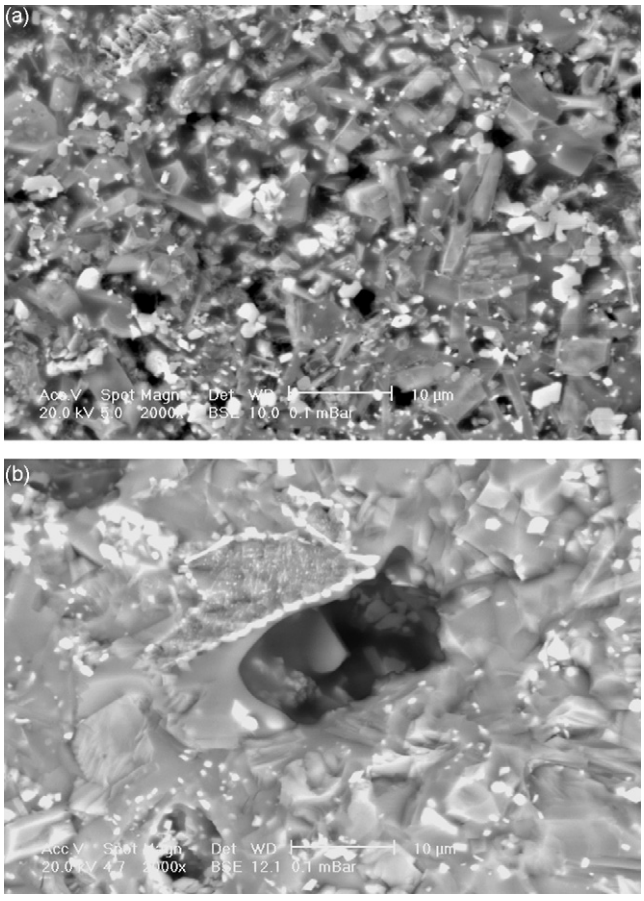

Fig. 6. BSE-SEM images of final material, obtained after 1 h at 1100 °C: surface (a) and fracture (b).

The dilatometric and pycnometric results highlight that the studied tuffs are characterized by a narrow sintering interval of 20–30 °C with optimal densification temperature of ~1100 °C (i.e. close to the liquidus temperature). This behaviour can be explained by the partial melting of formed crystal phases between the solidus and liqudus temperatures. At lower temperatures (i.e. at 1040–1060 °C), the amount of liquid phase in the sample is small, its viscosity is high and the densification is scarce. On the contrary, at high temperatures (i.e. at 1140 °C) the percentage of melt in the sample increases substantially, which results in deformation and swelling.

The relationship between sintering behaviour and phase formation was studied by XRD analysis and the obtained results are presented in Fig. 4. The spectrum of parent tuffs is shown in Fig. 4a, while Figs. 4b and 4c present the spectra of samples quenched in water after heating at 10 °C/min up to 1000 and 1100 °C, respectively. Figs. 4d and 4e show the spectra of specimens sintered for 1 h at 1100 °C: the first sample is quenched in water, whereas the second one is cooled at 10 °C/min. In order to elucidate better the variations in crystallinity, the spectrum of basalt glass, obtained after re-melting of the tuffs at 1350 °C and quenching in water, is plotted together with ones of the studied samples.

The spectrum of parent tuffs shows mainly amorphous phase and 19 ± 6 wt.% crystal phase made by pyroxene, plagioclases

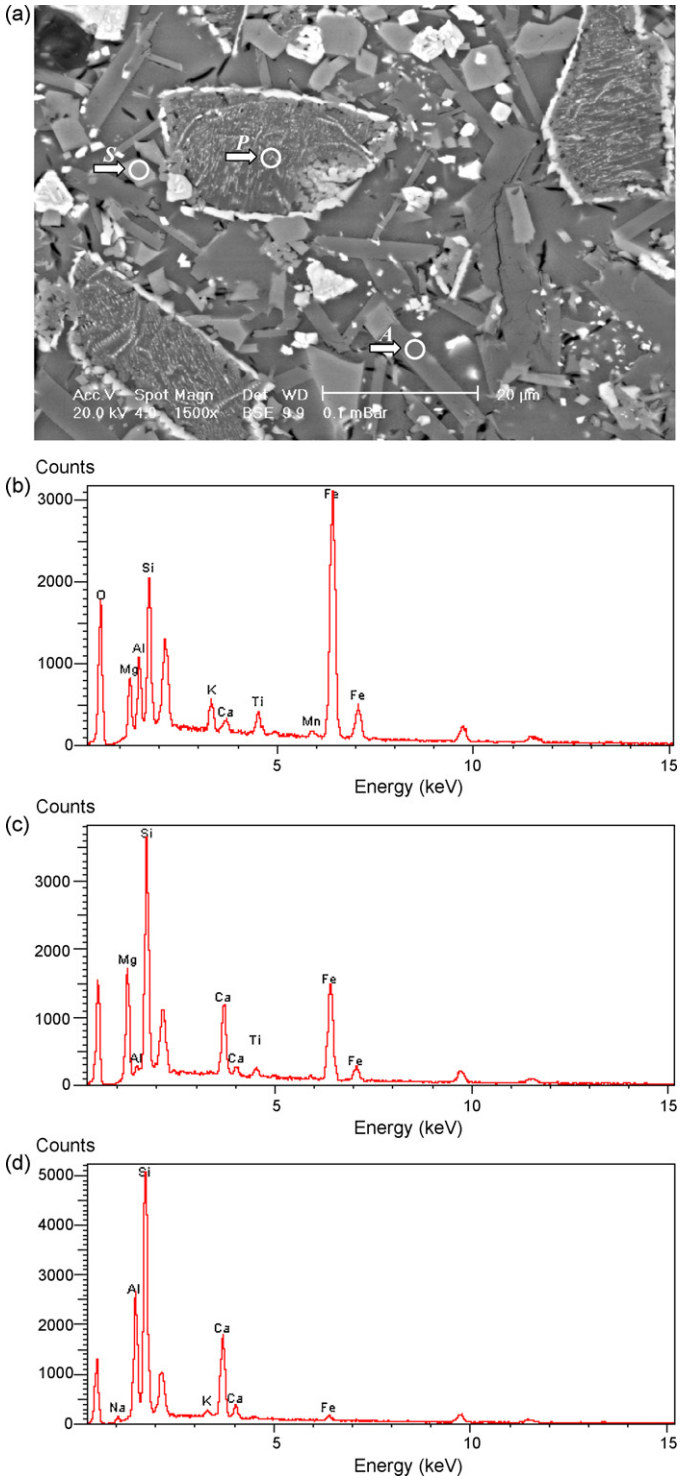

Fig. 7. BSE-SEM image of polished final sample (a) and EDS analysis of the main crystal phases in the material: spinel (b), pyroxene (c) and anorthite (d).

(anorthite solid solution), olivine (forsterite solid solution) and spinel.

Because of secondary crystallization during the heat-treatment the amount of residual glassy phase decreases significantly. As a result, the sample, heated up to 1000 °C (spectrum 4b), evidences crystallinity of 47 ± 4% and shows

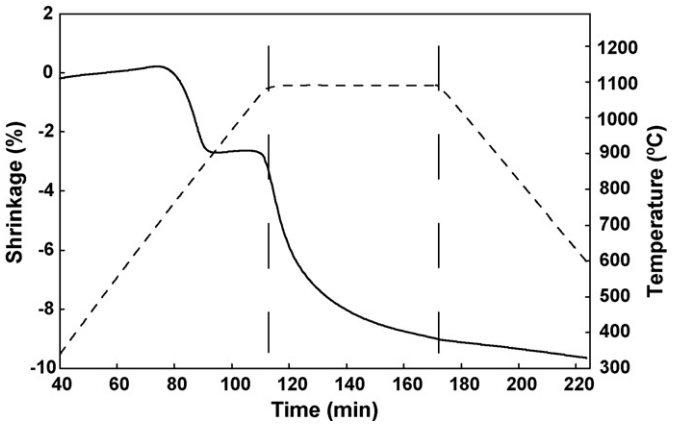

Fig. 8. Sintering traces vs. time, obtained at 10 °C/min heating and cooling rate and 1 h soaking at 1090 °C.

formation of new spinels and pyroxenes, as well as beginning of hematite crystallization.

The sample, heated up to the sintering temperature of 1100 °C (spectrum 4c), contains 39 ± 6% crystal phase. It is observed that the amounts of olivine and pyroxene decrease, while that of hematite increases. After 1 h sintering at 1100 °C (spectrum 4d), the olivine phase significantly decreases, while the content of the other crystal phases remains similar to that in spectrum 4c.

The final sample (sintered for 1 h at 1100 °C and cooled at 10 °C/min) is characterised by an increased crystallinity of 61 ± 5%, which indicates that about 20% crystal phase (plagioclase, spinels and pyroxene) is formed during the cooling step. Similar XRD spectrum was also obtained at cooling rate of 2 °C/min, which confirms the high crystallization trend of studied tuffs.

3.2. Structure and properties

The structure of final material, which was sintered at 1100 °C, was studied by SEM. Figs. 5a and 5b show SEM images of sam-

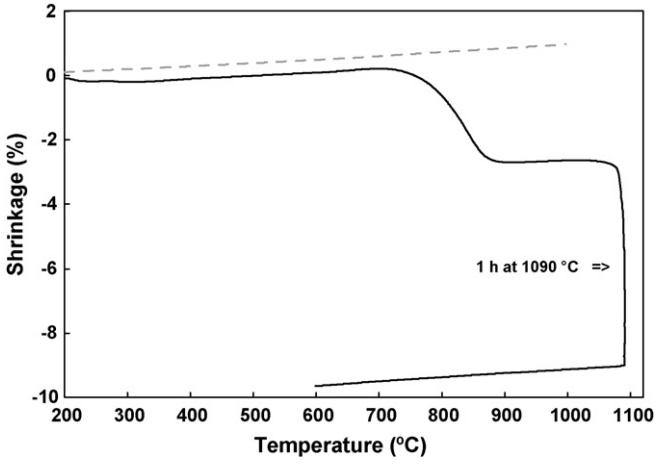

Fig. 9. Sintering traces vs. temperature, obtained at 10 °C/min heating and cooling rate and 1 h soaking at 1090 °C and dilatometric traces of the final sample, obtained at heating and cooling rates 10 °C/min.

Table 1
Properties of final material from sintered tuffs (ST), "classical" petrurgical products (P), tiling ceramics (C) and building glass-ceramics (GC)

Property	ST	P	C	GC
Water absorption (%)	<0.03%	<0.2	0–4	–
Density (g/cm^3)	2.66 ± 0.01	2.8–3	2.3–2.5	2.7–2.9
Young modulus (GPa)	93.3 ± 3.3	60–90	50–70	50–120
Bending strength (MPa)	100.5 ± 5.6	45–100	30–60	50–130
Coefficient of linear thermal expansion ($\times 10^{-7}$ K^{-1})	85.4	80–100	55–75	50–80

ple surface and fracture, respectively, and demonstrate the lack of open porosity in the surface and the presence of moderate closed porosity in the bulk. The corresponding EDS analysis (Fig. 5c for the surface and Fig. 5d for the fracture, respectively) evidence an increase of Fe and Ca content in the surface layer, which is a consequence of the Fe^{2+} oxidation on grain surface.[35–37] In fact, the unpolished sintered samples have reddish colour, while after grinding and polishing the colour becomes dark brown.

These results suggest that some differences between "surface" and "bulk" structures can be expected, and that the hematite is formed mainly on the grains surface. Fig. 6 shows images of the surface (Fig. 6a) and the fracture (Fig. 6b) obtained by BSE technique. It is evidenced that the surface is characterized by a more fine-crystalline morphology, while larger crystals and pores with rough and indented crystalline surface are observed in the sample bulk.

Fig. 7a shows a BSE image obtained after polishing (final treatment with 1 μm diamond paste) and etching (3 s with 2 wt.% HF). Here the high crystallinity of sample, as well as the presence of different crystal phases is clearly visible. The corresponding EDS spectra of formed spinel, *S*, pyroxene, *P*, and plagioclase (anorthite s.s.), *A*, are presented in Fig. 7b–d, respectively.

The relatively high percentage closed porosity, as well as the coarse polycrystalline surface of formed pores, are unusual for a well sintered traditional ceramic and indicate a possible formation of crystallization induced porosity, P_{CR},[38] during the sintering and cooling steps.

This kind of porosity is a result of the volume changes, accompanying the crystallization process; its formation could be expected mainly at high crystallinity and at crystal phases with an elevated crystallization volume variation.

In an attempt to verify the hypothesis for P_{CR} formation some additional dilatometric measurements, which analyse the shrinkage of samples during the sintering and cooling steps, were conducted. Fig. 8 shows sintering traces, obtained at heating and cooling rate of 10 °C/min, and 1 h held at 1090 °C as a function of sintering time. Fig. 9 shows the same plot as a function of temperature (solid line), together with the dilatometric traces of the final sintered sample at the same heating and cooling rate (dashed line).

Pycnometric measurements demonstrated that the crystallization process during cooling (after 1 h sintering at 1100 °C) increases the absolute density from 2.824 g/cm^3 (for quenched in water sample) to 2.876 g/cm^3 (for cooled at 10 °C/min sample). This difference is in a good agreement with the formation of about 20 wt.% crystal phase, made by plagioclase, pyroxene and spinels.[39] If this volume variation is transformed in linear shrinkage an additional value of ∼0.6% $\Delta L/L_0$ can be expected, whereas if it provokes P_{CR} formation the closed porosity of sample can increase by ∼2%.

Figs. 8 and 9 demonstrate the lack of crystallization shrinkage at the cooling step and identical linear thermal expansion of both samples (i.e. during cooling after the sintering step and during heating and subsequent cooling of the final material). These results elucidate that the volume variation, related to the phase formation during the cooling could lead to formation of crystallization induced porosity.

The crystallization induced porosity is different from the residual inter-granular porosity in the ceramics, which significantly decreases their mechanical properties. It is supposed that the P_{CR} formation leads to relaxation of the crystallization induced stresses, which improves the mechanical characteristics of materials.[38]

The properties of final product are summarized in Table 1, together with these of tiling ceramics,[40] petrurgical products,[2,3] obtained by re-melting of basaltic rocks, and building glass-ceramic materials.[33]

The new material is characterized by a moderate density, thermal expansion, which is similar to the traditional building materials, and zero water absorption. At the same time, notwithstanding of its simple and low-cost manufacture cycle, the mechanical characteristics significantly surpass these of the traditional ceramics (sintered at 100–150 °C higher temperatures) and are comparable to these of the glass-ceramics and "classical" petrurgical materials (which, however, are obtained by glass melting and longer crystallization heat-treatment).

4. Conclusions

Well sintered material is obtained after milling of alkaline basaltic tuffs below 75 μm, pressing at 100 MPa and sintering at 1100 °C (i.e. near to the liquidus temperature).

The final samples are characterized by zero water absorption, 8–9 vol.% closed porosity and structure similar to that of a glass-ceramic material.

Due to the high crystallization trend of used composition, phase formation takes place during the sintering and cooling stages. As a result, the new material is characterized by high crystallinity of ∼65% and very good mechanical properties: Young modulus of 90 GPa and bending strength of 100 MPa.

Acknowledgments

The authors gratefully acknowledge the financial support within Project TK-X-1713/07 (Bulgarian Ministry of Science and Education). They express sincere thanks to Prof. M. Pelino (University of L'Aquila) for the immense technical support, Dr. E. Bernardo (University of Padova) for the evaluations of mechanical properties and Dr. G. Taglieri (University of L'Aquila) for the XRD analysis.

References

1. Locsei, B., *Molten Silicates and their Properties*. Akademiai Kiado, Budapest, 1970.
2. www.petrurgia.bg.
3. www.eutit.cz.
4. www.basfiber.com.
5. www.abresist.com.
6. Bickford, D. F. and Jantzen, C. M., Devitrification of defense nuclear waste glass: role of melt insolubles. *J. Non-Cryst. Solids*, 1986, **84**, 299–307.
7. Donald, I. W., Metcalfe, B. L. and Taylor, R. N. J., Review—the immobilization of high level radioactive wastes using ceramics and glasses. *J. Mater. Sci.*, 1997, **32**, 5851–5887.
8. Ojovan, M. I. and Lee, W. E., *New Development in Glassy Nuclear Wasteforms*. Nova Scientific Publisher, New York, 2007.
9. Romero, M. and Rincon, J. Ma, Preparation and properties of high iron oxide content glasses obtained from industrial wastes. *J. Eur. Ceram. Soc.*, 1998, **18**, 153–160.
10. Karamanov, A., Pisciella, P., Cantalini, C. and Pelino, M., Influence of the Fe^{3+}/Fe^{2+} ratio on the crystallization of iron-rich glasses made with industrial wastes. *J. Am. Ceram. Soc.*, 2000, **81**, 3153–3157.
11. Scarinci, G., Brusatin, G., Barbieri, L., Corradi, A., Lancellotti, I., Colombo, P., Hreglich, S. and Dalligna, R., Vitrification of industrial and natural wastes with production of glass fibres. *J. Eur. Ceram. Soc.*, 2000, **20**, 2485–2490.
12. Karamanov, A. and Pelino, M., Crystallization phenomena in iron rich glasses. *J. Non-Cryst. Solids*, 2001, **281**(1–3), 139–151.
13. Kavouras, P., Komninou, P. and Chrissafis, K., Microstructural changes of processed vitrified solid waste products. *J. Eur. Ceram. Soc.*, 2003, **23**, 1305–1311.
14. Francis, A. A., Rawlings, R. D. and Sweeney, R., Crystallization kinetic of glass particles prepared from a mixture of coal ash and soda-lime cullet glass. *J. Non-Cryst. Solids*, 2004, **333**, 187–193.
15. Surensen, P. M., Pind, M., Yue, Y. Z., Rawlings, R. D., Boccaccini, A. R. and Nielsen, E. R., Effect of the redox state and concentration of iron on the crystallization behavior of iron-rich aluminosilicate glasses. *J. Non-Cryst. Solids*, 2005, **351**, 1246–1253.
16. Karamanov, A., Aloisi, M. and Pelino, M., Vitrification of copper flotation waste. *J. Hazard. Mater.*, 2007, **140**, 333–339.
17. Kavouras, P., Kehagias, T., Tsilika, I., Kaimakamis, G., Chrissafis, K., Kokkou, S., Papadopoulos, D. and Karakostas, Th., Glass-ceramic materials from electric arc furnace dust. *J. Hazard. Mater.*, 2007, **A139**, 424–429.
18. Znidarsic-Pongarac, V. and Kolar, D., The crystallization of diabase glass. *J. Mater. Sci.*, 1991, **26**, 2490–2494.
19. Yılmaz, S., Ozkan, O. T. and Gunay, V., Crystallization kinetics of basalt glass. *Ceram. Int.*, 1996, **22**, 477–481.
20. Rincon, J. Ma., Càceres, J., Gonzàles-Oliver, C. J., Russo, D. O., Petkova, A. and Hristov, H., Thermal and sintering behaviour of basalt glasses and natural basalt powders. *J. Therm. Anal. Calorim.*, 1999, **56**, 931–938.
21. Abdel-Hameed, S. A. M. and Bakr, I. M., Effect of alumina on ceramic properties of cordierite glass–ceramic from basalt rock. *J. Eur. Ceram. Soc.*, 2007, **27**, 1893–1897.
22. Garbonchi, G., Dondi, M., Morandi, N. and Tateo, F., Possible use of altered volcanic ash in ceramic tile production. *Ind. Ceram.*, 1999, **19**, 67–74.
23. Ergul, S., Akyildiz, M. and Karamanov, A., Ceramic material from basaltic tuffs. *Ind. Ceram.*, 2007, **37**, 75–80.
24. Bayrak, G. and Yilmaz, S., Crystallization kinetics of plasma sprayed basalt coatings. *Ceram. Int.*, 2006, **32**, 441–446.
25. Morse, S. A., *Basalts and Phase Diagrams*. Springler-Verlag, New York/Heidelberg/Berlin, 1982.
26. Càceres, J., Hernàndes, G. and Rincon, J. Ma., Characterization of fibers as rockwool for insulation obtained from canary islands basalts. *Materiales de Consrucción*, 1996, **46**, 242–243.
27. Beall, H. and Rittler, H. L., Basalt glass ceramics. *Ceram. Bull.*, 1976, **55**, 579–582.
28. Rincon, J. Ma., Pelino, M. and Romero, M., Glass-ceramics obtained from axial pressing and sintering of vitrified high iron content red mud. In *Proceedings of the 1st National Congress on Valorization and Recycling of Industrial Wastes*, 1997, pp. 169–181.
29. Karamanov, A., Taglieri, G. and Pelino, M., Sintering behavior and properties of iron-rich glass-ceramics. *J. Am. Ceram. Soc.*, 2004, **87**, 1571–1574.
30. Karamanov, A., Taglieri, G. and Pelino, M., Sintering in nitrogen atmosphere of iron-rich glass-ceramics. *J. Am. Ceram. Soc.*, 2004, **87**, 1354–1357.
31. Karamanov, A., Ergul, S., Akyildiz, M. and Pelino, M., Sinter-crystallization of a glass obtained from basaltic tuffs. *J. Non-Cryst. Solids*, 2008, **354**, 290–295.
32. Bilgin, A. Z. and Ercan, T., Petrology of the quarternary basalts of Iskenderun Gulf-Osmaniye area. *Geol. Soc. Turkey Bull.*, 1981, **24**, 21–30.
33. Strnad, Z., *Glass-Ceramic Materials*. Elsevier, Amsterdam, 1986.
34. Kim, H. S., Rawlings, R. D. and Roger, P. S., Quantitative determination of crystalline and amorphous phases in glass-ceramics by X-ray diffraction analysis. *Br. Ceram. Trans. J.*, 1989, **88**, 21–25.
35. Cooper, R. D., Fanselow, J. B. and Poker, D. B., The mechanism of oxidation of a basaltic glass: Chemical diffusion of network-modifying cations. *Geochimica et Cosmochimica Acta*, 1996, **60**, 3253–3265.
36. Pelino, M. and Karamanov, A., Reply to "Comment on "The influence of the Fe^{3+}/Fe^{2+} ratio on the crystallization of iron-rich glasses from industrial wastes". *J. Am. Ceram. Soc.*, 2001, **84**, 2742–2743.
37. Burkhard, D. J. M. and Scherer, T., Surface oxidation of basalt glass/liquid. *J. Non-Cryst. Solids*, 2006, **352**, 241–247.
38. Karamanov, A. and Pelino, M., Induced crystallization porosity and properties of sintered diopside and wollastonite glass-ceramics. *J. Eur. Ceram. Soc.*, 2008, **28**, 555–562.
39. Karamanov, A. and Pelino, M., Evaluation of the degree of crystallisation in glass-ceramics by density measurements. *J. Eur. Ceram. Soc.*, 1999, **19**, 649–654.
40. Hlavac, J., *The Technology of Glass and Ceramics: An Introduction*. Elsevier, Amsterdam, 1983.